Capture of negative muons by hydrogen atoms at low collision energies

Kazuhiro Sakimoto

Institute of Space and Astronautical Science, Japan Aerospace Exploration Agency, Yoshinodai, Sagamihara 229-8510, Japan

(Received 26 October 2009; published 29 January 2010)

A rigorous quantum mechanical calculation is carried out for negative muon capture by atomic hydrogen ($\mu^- + \mathrm{H} \rightarrow \mu^- p + e$) by using the R-matrix method. The total and final-state selected capture cross sections are calculated at low collision energies ranging from 0.001 to 1 eV. The total capture cross section can, on average, be explained in terms of a previously obtained empirical formula [K. Sakimoto, Phys. Rev. A **66**, 032506 (2002)]. However, the present result exhibits additional undulation and cusp structures, which stem from quantum phenomena. The muons are predominantly captured into the highest energetically possible state of $\mu^- p$ in the present energy region. However, the $\mu^- p$ products having high angular momenta cannot be formed unless the collision energy becomes high.

DOI: 10.1103/PhysRevA.81.012511 PACS number(s): 36.10.Ee, 36.10.Gv

I. INTRODUCTION

The three-body problem of collisions between a point charge and a H atom is of fundamental dynamical importance. We can investigate the special case that the point charge is negative and yet heavy by considering hadrons and leptons such as antiprotons ($\bar{p}$), kaons (K^-), muons (μ^-), and pions (π^-). Then, the most remarkable event in the slow collisions is that the heavy negative particles (X^-) are captured to form exotic atoms $X^- p$, which are a bound hydrogenic system. This is also an important process for making the exotic atoms. High-resolution spectroscopic experiments on the exotic atoms provide some of the most precise tests of QED effects [1,2] and the valuable information about strong interactions [3–6]. As a result of the large mass difference between X^- and e, very high-lying orbitals of $X^- p$ are mostly formed in the X^- capture by H. The energies and linewidths of X-ray radiation emitted in the subsequent cascade process of the highly excited exotic atoms are the important quantities to be measured in these studies. Therefore, it is absolutely necessary to get definite and reliable information on the level population of the exotic atoms formed in the capture. So far, many researchers introduced various kinds of collisional approximations to understand the dynamics of the capture reaction [7]. However, rigorous quantum mechanical (QM) calculations were carried out rather recently by using a time-dependent wave packet propagation method [8,9] and another type of time-dependent approach [10,11].

Unfortunately, if resonance phenomena are significant or collision energies are low, the time-dependent method requires an extremely time-consuming computation and hence cannot be regarded as appropriate. Very recently, time-independent QM calculations were carried out for the $\bar{p}$ and μ^- captures by He^+ ions [12,13]. Because the calculation was based on an R-matrix method [14], we were able to closely investigate a huge number of resonances characteristic of these systems. In the present article, we use the R-matrix method to investigate the low-energy behavior of the μ^- capture by H

$$\mu^- + \mathrm{H}(1s) \rightarrow \mu^- p(N, L) + e, \tag{1}$$

where $\mu^- p$ is called the muonic hydrogen and (N, L) are the associated principal and angular momentum quantum numbers. Although the muon is an unstable particle, its lifetime ($\sim 2.2 \times 10^{-6}$ s) is much longer than a time scale of the capture process. In contrast with hadrons, it is a very good approximation to regard the muon as a structureless point charge in the present study. The previous QM calculations [9,11] were carried out for the μ^- capture by H only if the collision energy was $E \geqslant 1$ eV. Here, we calculate the total and final-state selected capture cross sections further at lower collision energies ranging from 1 down to 0.001 eV.

The capture channels $N = 0 - 13$ are energetically open even in the limit as $E \rightarrow 0$ and the channel $N = 14$ becomes additionally open when $E > 0.705$ eV (Fig. 1). For slow μ^-+ H collisions, the adiabatic (Born-Oppenheimer) approximation is the most suitable way to characterize the dynamical features if the relative distance is much larger than the so-called Fermi-Teller distance $R_{\mathrm{FT}} = 0.639$ au [8,9,15,16]. Figure 1 shows the effective potentials of the μ^-+ H system in the lowest (1σ) adiabatic state for the total angular momentum quantum numbers $J = 0 - 15$. Because the interaction range is <2 au for the capture reaction [8,9], we can see that the total angular momentum of $J \geqslant 14$ has a negligible contribution to the reaction if the collision energy is $E \leqslant 1$ eV. In a previous study [17], the R-matrix calculation was already performed for the same μ^--p-e system although the object of concern was the inverse process of Eq. (1) [i.e., $e + \mu^- p \rightarrow \mu^-$+ H, which may be called dissociative attachment (DA)]. Only a restricted range of total angular momenta (i.e., $J = 7 - 16$) were associated with the DA process for the high initial $\mu^- p$ states of $N = 13$, 14, and 15 and $L \geqslant 9$ [17]. To obtain the capture cross sections here we need further to perform the R-matrix calculation for $J = 0 - 6$.

The details of the R-matrix formulation and the numerical method for the application to the capture of heavy negative particles are described elsewhere [12,13]. Hence, in Sec. II we give only a short summary of the R-matrix method. In Sec. III A, the capture probability for each total angular momentum J is presented and a discussion on some QM effects (peak and cusp structures) is conducted. Section III B gives the results of the total capture cross section obtained by summing over all the final states. In Ref. [9], from the QM results calculated at high collision energies ($E \geqslant 5.5$ eV), an empirical law was derived for the relation between the total

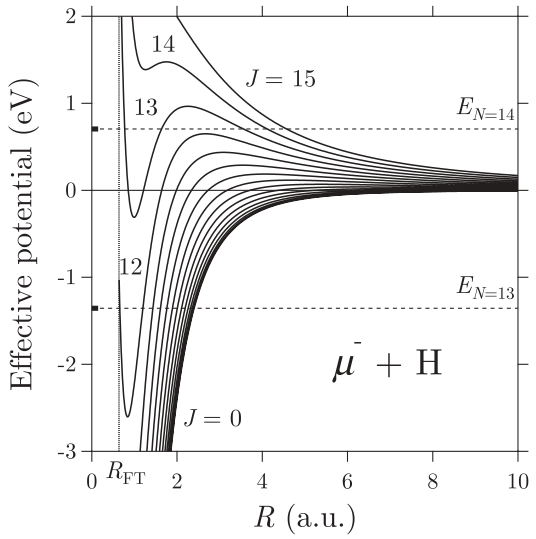

FIG. 1. The sum of the centrifugal and 1σ adiabatic potentials of the $\mu^- + \mathrm{H}$ system as a function of the relative distance R for the total angular momentum quantum numbers $J = 0 - 15$. The $\mu^- p$ energy levels E_N are indicated by horizontal dashed lines. The energies are measured from the ground-state energy of H. The vertical line labeled R_{FT} represents the Fermi-Teller distance.

capture probability and the classical turning point associated with the 1σ adiabatic potential. The applicability of this empirical law is examined for the low-energy collisions. In Sec. III C, the final-state selected capture cross sections are presented.

II. THEORY AND CALCULATION

The time-independent Schrödinger equation for the total system is

$$\tilde{H}\Psi_\tau^{JM\kappa} = E_{\mathrm{tot}}\Psi_\tau^{JM\kappa}, \tag{2}$$

where (J, M) are the total angular momentum quantum numbers, κ is the total parity, E_{tot} is the total energy, and τ indicates an initial collision channel. The Hamiltonian operator $\tilde{H}$ is given by

$$\tilde{H} = -\frac{1}{2m_R R}\frac{\partial^2}{\partial R^2}R + \frac{\tilde{\mathbf{L}}^2}{2m_R R^2} - \frac{1}{2m_r r}\frac{\partial^2}{\partial r^2}r + \frac{\tilde{\mathbf{l}}^2}{2m_r r^2} + V, \tag{3}$$

where m_R, $\mathbf{R}$, and $\tilde{\mathbf{L}}$ are, respectively, the reduced mass, the relative position vector, and the angular momentum vector (operator) of the $\mu^- + p$ system; m_r, $\mathbf{r}$, and $\tilde{\mathbf{l}}$ are the corresponding quantities for the electron in $\mu^- p + e$, as described by the Jacobi coordinates, and V is the sum of the Coulomb potentials. Here and in the following, we use au unless otherwise stated.

If the total energy is far below the excited-state energy of H, the possible channel of the reactant $\mu^- + \mathrm{H}$ is only the 1σ adiabatic electronic state [8,9,17]. In this case, the total parity must be $\kappa = (-1)^J$. The collision energy of $\mu^- + \mathrm{H}$ is given by $E = E_{\mathrm{tot}} - \epsilon_{1s}$, where $\epsilon_{1s} = -0.5$ au is the ground-state energy of H. The capture (or electron emission) channel $\mu^- p + e$ is identified by the principal and angular momentum quantum numbers (N, L) of the hydrogenic system $\mu^- p$ and the electronic angular momentum quantum number l [17]. The energy of $\mu^- p$ is given by

$$E_N = -\frac{m_R}{2N^2}. \tag{4}$$

To solve the collision problem we employ the R-matrix method [14,17]. We define the inner region by $0 \leqslant R \leqslant A$ and $0 \leqslant r \leqslant a$ and consider there the R-matrix eigenvalue equation

$$[\tilde{H} + \tilde{L}_{\mathrm{B}}]\Phi_\rho^{JM\kappa}(\mathbf{R}, \mathbf{r}) = E_\rho^{J\kappa}\Phi_\rho^{JM\kappa}(\mathbf{R}, \mathbf{r}), \tag{5}$$

where

$$\tilde{L}_{\mathrm{B}} = \frac{1}{2m_R A}\delta(R - A)\frac{\partial}{\partial R}R + \frac{1}{2m_r a}\delta(r - a)\frac{\partial}{\partial r}r, \tag{6}$$

is the Bloch operator [18] and ρ identifies the discrete eigenvalues $E_\rho^{J\kappa}$. For the solution of Eq. (5), the wave function $\Phi_\rho^{JM\kappa}$ is expanded in the form [17]

$$\Phi_\rho^{JM\kappa}(\mathbf{R}, \mathbf{r}) = (Rr)^{-1}\sum_\lambda D_{M\lambda}^{J\kappa}(\hat{\mathbf{R}})\phi_\rho^{J\kappa\lambda}(R, r, \theta), \tag{7}$$

where $D_{M\lambda}^{J\kappa}(\hat{\mathbf{R}})$ is the parity-specified Wigner D function normalized to unity, θ is the angle between $\mathbf{R}$ and $\mathbf{r}$, and $\lambda(\geqslant 0)$ is the electronic magnetic quantum number projected onto $\hat{\mathbf{R}}$. The wave function $\phi_\rho^{J\kappa\lambda}(R, r, \theta)$ was calculated using a direct numerical algorithm based on grid (discrete-variable) representation [12,13,17]. The R-matrix calculation was already completed for $J \geqslant 7$ in the previous DA study [17]. Here, we further carried out the calculation for the low angular momenta $J = 0 - 6$. As in the previous study [17], we took the boundary values $A = 3$ and $a = 10$ au, included the channels of $\lambda \leqslant 1$ and $l \leqslant 4$, and chose the numbers of grid points $(N_r, N_\theta) = (35, 10)$ in the (r, θ) coordinates. For the low J, however, the number of grid points N_R in the R coordinate must be taken to be larger than the previous value ($N_R = 30$): In the present calculation, we chose $N_R = 100$ for $J = 0$, $N_R = 70$ for $J = 1$, $N_R = 60$ for $J = 2$, $N_R = 50$ for $J = 3$, $N_R = 40$ for $J = 4$ and 5, and $N_R = 30$ for $J = 6$.

Once we solve Eq. (5) we can define the R matrix at the boundary ($R = A$ and $r = a$); its elements are identified by the collision channel 1σ or (N, L, l) [17]. We must further propagate the R matrix from $r = a$ to a larger distance r_{max} to eliminate the long-range coupling effects in the electron emission channel. If $E < E_{N=14} - \epsilon_{1s} = 0.705$ eV, the emitted electrons always have kinetic energies higher than $\epsilon_{1s} - E_{N=13} = 1.36$ eV (Fig. 1). In this case, the value of $r_{\mathrm{max}} = 20$ au, smaller than those chosen in Ref. [17], was found to be sufficient. To extract the S-matrix elements associated with the reactant channel, the regular and irregular solutions for the 1σ adiabatic potential must be known at $R = A$. These two reference functions at low collision energies were determined by the backward propagation of the corresponding Wentzel-Kramers-Brillouin (WKB) solutions given at $R = 40$ au. In these ways we can calculate the scattering S-matrix elements $S_{NLl,1\sigma}^{J\kappa}$ for the capture reaction.

The probability of the capture into the (N, L, l) product channel is given by

$$P^{J\kappa}(N, L, l) = \left|S_{NLl,1\sigma}^{J\kappa}\right|^2. \tag{8}$$

We define the total capture probability summed over all the final channels by

$$P^{J\kappa} = \sum_{NLl} P^{J\kappa}(N, L, l), \tag{9}$$

and the final-state selected capture probabilities by

$$P^{J\kappa}(N, L) = \sum_{l} P^{J\kappa}(N, L, l), \tag{10}$$

$$P^{J\kappa}(N) = \sum_{Ll} P^{J\kappa}(N, L, l), \tag{11}$$

$$P^{J\kappa}(L) = \sum_{Nl} P^{J\kappa}(N, L, l), \tag{12}$$

$$P^{J\kappa}(l) = \sum_{NL} P^{J\kappa}(N, L, l). \tag{13}$$

The total capture cross section is

$$\sigma = \frac{\pi}{2m_R E} \sum_{J\kappa} (2J+1) P^{J\kappa}. \tag{14}$$

In the same way, we can define the final-state selected capture cross sections $\sigma(N, L)$, $\sigma(N)$, $\sigma(L)$, and $\sigma(l)$.

III. RESULTS AND DISCUSSION

A. Capture probabilities

We show in Fig. 2 all the present results of the total capture probabilities $P^{J\kappa}$ that have nonnegligible values at collision energies $E \leqslant 1$ eV. Because the probability is multiplied by the weight factor $2J+1$, the importance of each partial wave (J) in the cross section [cf. Eq. (14)] can be evaluated directly from the figure. One of the most remarkable results is that there is a cusp structure at $E \simeq 0.7$ eV. This anomaly is the threshold effect: A new capture channel $\mu^- p(N = 14) + e$ starts at the collision energy $E = E_{N=14} - \epsilon_{1s} = 0.705$ eV. Because the product $\mu^- p$ has the hydrogenic degeneracy and furthermore

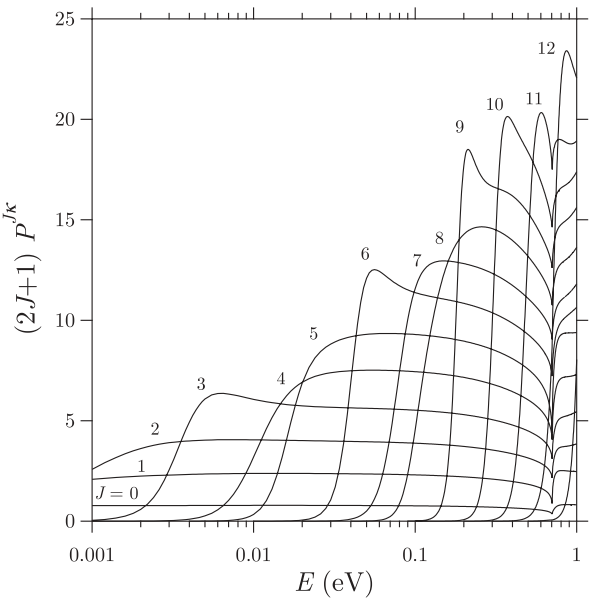

FIG. 2. Weighted capture probabilities $(2J+1)P^{J\kappa}$ as a function of the collision energy E for the total angular momenta $J = 0 - 13$.

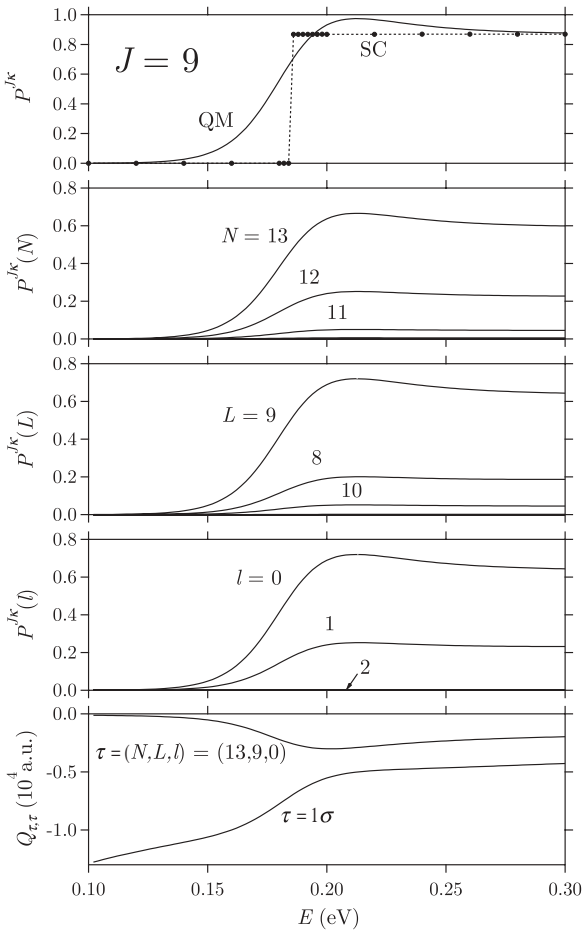

FIG. 3. Capture probabilities $P^{J\kappa}$, $P^{J\kappa}(N)$, $P^{J\kappa}(L)$, $P^{J\kappa}(l)$, and time delays $Q_{\tau,\tau}$ with $\tau = (N, L, l) = (13, 9, 0)$ and 1σ (see text) as a function of the collision energy E for the total angular momentum $J = 9$. The total capture probabilities obtained by the SC method [9] are also shown in the uppermost graph.

the long-range dipole interaction works between $\mu^- p$ and e, there can be asymptotically an attractive effective potential, which is proportional to $-1/r^2$. In such a case, the threshold anomaly becomes prominent [17,19,20] and hence we can see a clear cusp structure. The appearance of the cusp is evidently a QM effect.

Another interesting feature is that several partial waves have a seemingly peak-like structure (e.g., at energies $E \simeq 0.0065$ eV for $J = 3$, $E \simeq 0.056$ eV for $J = 6$, $E \simeq 0.21$ eV for $J = 9, \ldots,$). Here, we specifically examine the $J = 9$ partial wave. Figure 3 shows the capture probabilities $P^{J\kappa}$, $P^{J\kappa}(N)$, $P^{J\kappa}(L)$, and $P^{J\kappa}(l)$ for $J = 9$ at energies $0.1 \leqslant E \leqslant 0.3$ eV. It is found that the peak-like structure at $E \simeq 0.21$ eV is observed mainly in the capture channels of $N = 13$, $L = J = 9$, and $l = 0$. The total capture probabilities are compared with those obtained by using the semiclassical (SC) method [9], in which the relative radial motion is treated by classical mechanics and the other motions are by quantum mechanics. The $J = 9$ effective potential has a barrier height of 0.186 eV at $R = 4.06$ au (Fig. 1). The barrier penetration is forbidden in classical mechanics and hence the SC probabilities form a step function of E. In contrast, the complete QM calculation shows a smooth variation with E in the vicinity of

$E = 0.186$ eV. Because the SC probabilities are nearly constant at $E > 0.186$ eV, the peak-like structure of the QM results is emphasized by comparison with the SC results. It seems that the peak originates from a QM effect (possibly a resonance). As was discussed in Ref. [17], since the peak position is not just below the $N = 14$ channel threshold ($= 0.705$ eV) it cannot be a Feshbach-type resonance. Then, a likely candidate is the resonance associated with the shape of the effective potential. However, the resonance state cannot be a usual quasibound motion because the peak position is above the barrier height. A previous study of chemical reaction [21] shows that a resonance can result from the presence of a reaction barrier even if the energy is above the barrier height. To explore this possibility in the present case we calculate the scattering time-delay matrix $\mathcal{Q} = -i(d\mathcal{S}/dE)\mathcal{S}^\dagger$ [22], with $\mathcal{S}$ being the S matrix. The diagonal element $Q_{\tau,\tau}$ has the meaning of the average time delay of the collisions from the initial channel τ. Figure 3 also includes the time delays for the incident channel $\tau = 1\sigma$ and the capture channel $\tau = (N, L, l) = (13, 9, 0)$. We can find no remarkable structure except for a vague one near the energy corresponding to the barrier height. Therefore, we must say that the peak at $E \simeq 0.21$ eV is related to no meaningful resonance. Also for the other peaks, their positions are above the barrier heights and the same conclusion is reached. In this study we cannot give a satisfactory explanation for the peak-like structure.

B. Total capture cross sections

The present results of the total capture cross section σ summed over all the final channels (N, L, l) are shown as a function of the collision energy E in Fig. 4. The cusp structure due to the $N = 14$ threshold effect is also still clearly observed in the total cross section. The peak-like structures

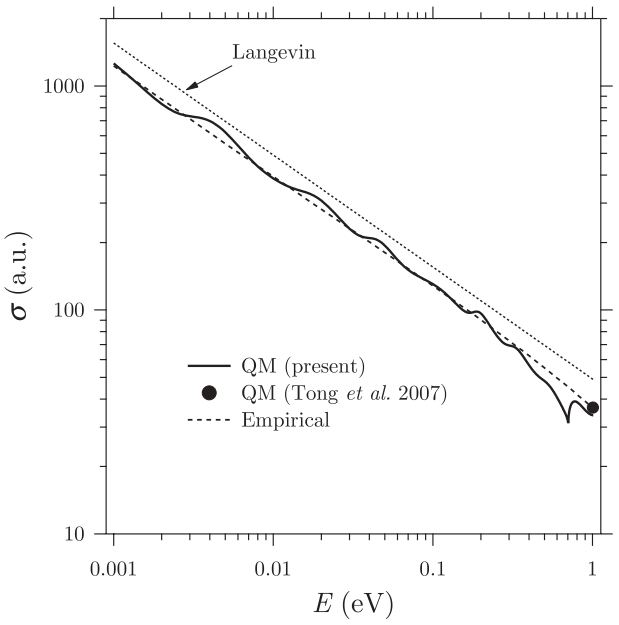

FIG. 4. Total capture cross sections as a function of the collision energy E obtained by the present QM calculation, by the QM calculation of Tong *et al.* [11], and by using the empirical formula ($\sigma_{\rm em}$). The Langevin cross section $\sigma_{\rm L}$ is plotted for comparison.

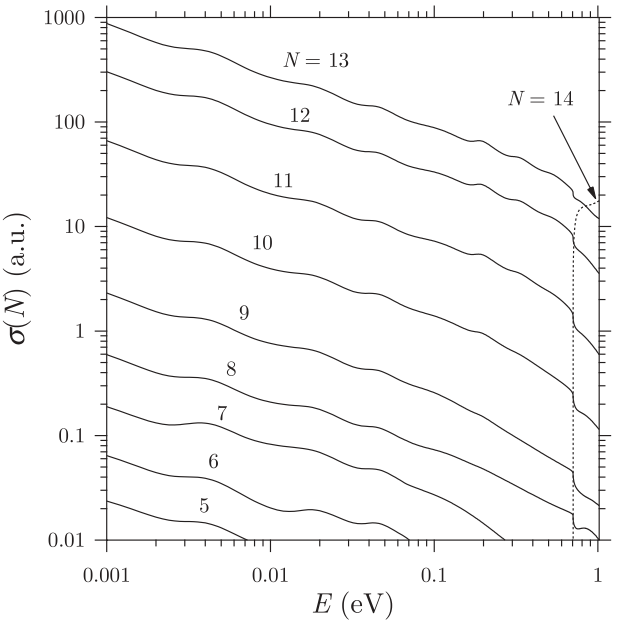

FIG. 5. N-state selected capture cross sections $\sigma(N)$ as a function of the collision energy E.

in several partial waves, together with the cusp structure, show the appearance of undulation in the variation of the total cross section with energy. The QM result calculated by Tong *et al.* [11] is available at $E = 1$ eV, which is the lowest energy in their study and is shown in the figure. The present result is slightly smaller than their value. The collision energy $E = 1$ eV is just above the $N = 14$ channel threshold 0.705 eV. In such a case, as seen later (cf. Fig. 5), most of the emitted electrons have very small kinetic energies. Therefore, the value of $r_{\rm max} = 20$ au chosen in the present calculation might not be large enough for the elimination of the long-range coupling effect [17]. It should be mentioned, furthermore, that Tong *et al.* [11] used the Jacobi coordinates associated with the $\mu^- + {\rm H}$ arrangement throughout their whole calculation. Their choice of Jacobi coordinates is evidently inappropriate for the description of the capture channel $\mu^- p + e$, though the error might not be so serious if the distance between p and e were not too large [11]. These factors can cause some discrepancy between the two QM results at $E = 1$ eV.

In Ref. [9], by examining the QM results obtained at high energies ($E \geqslant 5.5$ eV), the present author proposed the following empirical formula

$$P_{\rm em} = \left[0.79 + 0.12\exp\left(\frac{-0.0868}{R_{\rm TP}}\right)\right]\exp[-0.236(R_{\rm TP})^{5.2}], \tag{15}$$

for the relation between the total capture probability $P_{\rm em}$ and the classical turning point $R_{\rm TP}$ in the R motion. The turning point $R_{\rm TP}$ is estimated from the 1σ adiabatic potential, which is assumed to be a pure Coulomb form if $R < R_{\rm FT}$. Using this formula, we can calculate the empirical capture cross section in the form

$$\sigma_{\rm em} = 2\pi \int_0^\infty P_{\rm em} b db, \tag{16}$$

TABLE I. Ratios of the empirical (σ_{em}) and Langevin (σ_L) cross sections.

E (eV)	0.001	0.01	0.1	1.0
σ_{em}/σ_L	0.79	0.79	0.82	0.74

where b is the impact parameter of $\mu^- +$ H. Figure 4 shows that Eq. (16) provides values very close to the QM results on the whole, but consistently fails to produce the cusp and undulation structures.

In the ion-molecule reaction as in the present capture process, the polarization potential may play a decisive role [9]. We also plot in Fig. 4 the so-called Langevin cross section $\sigma_L = \pi(2\alpha/E)^{1/2}$, with α being the polarizability of the H atom. The empirical cross section σ_{em} seems to be proportional to σ_L. In Table I, we can find that the ratio σ_{em}/σ_L is mostly constant, especially at very low energies. Therefore, the energy dependence of the total capture cross section can be explained basically in terms of the polarization potential at energies $\ll 1$ eV.

C. Final-state selected capture cross sections

The results of the final-state selected capture cross section $\sigma(N)$ plotted against E are shown in Fig. 5. If the collision energy is below 0.705 eV, the $\mu^- p$ products occupy predominantly the highest energetically possible state (i.e., $N = 13$) and the cross section $\sigma(N)$ is a monotonic function of N. This means that the low-energy capture leads mainly to the emission of slow electrons. This result is just the same as what we found for the μ^- capture by He^+ though the latter case exhibits complicated resonance features [13]. Around $E = 0.705$ eV, we can see that the cross sections $\sigma(N)$ for $N \leqslant 13$ have a stepwise structure. It is further found that the cross section $\sigma(N)$ for the new channel $N = 14$ rises abruptly from zero at energies just above $E = 0.705$ eV and becomes larger than the others at $E > 0.842$ eV. We can understand that the cusp structure seen in the total cross section σ originates from the combination of the sharp drop in $\sigma(N \leqslant 13)$ and the rapid increase in $\sigma(N = 14)$. The state selected cross sections $\sigma(N)$ for the μ^- capture by H were calculated at $E \geqslant 2$ eV by Tong *et al.* [11]. At $E = 2$ eV, they also obtained the same result that most populated was the highest energetically possible state. If $E \geqslant 4$ eV, however, they showed that the cross section $\sigma(N)$ reached the maximum value for some lower state N.

The final-state selected capture cross sections $\sigma(L)$ are shown in Fig. 6. Because the dominant channel of the electron emission is $l = 0$ and the contribution of $l \geqslant 2$ to the capture is always $\lesssim 1\%$ (cf. Fig. 3), we have $L \simeq J$. Accordingly, if we regard L as J, we can see that the functional form of $\sigma(L)$ against E has a similarity to that of $(2J+1)P^{J\kappa}$ except for the energy multiplier E^{-1} in Eq. (14). Every angular momentum in the range of $L \leqslant 12$ is energetically allowed in the capture at $E < 0.705$ eV. However, if the collision energy is low, only low angular momenta J can contribute to the collisions. Therefore, the $\mu^- p$ products having high $L \sim 12$ cannot be formed unless the energy becomes high. Figure 7 shows the angular momentum quantum number $L = L_0$ for which the cross section $\sigma(L)$ becomes the largest at the same

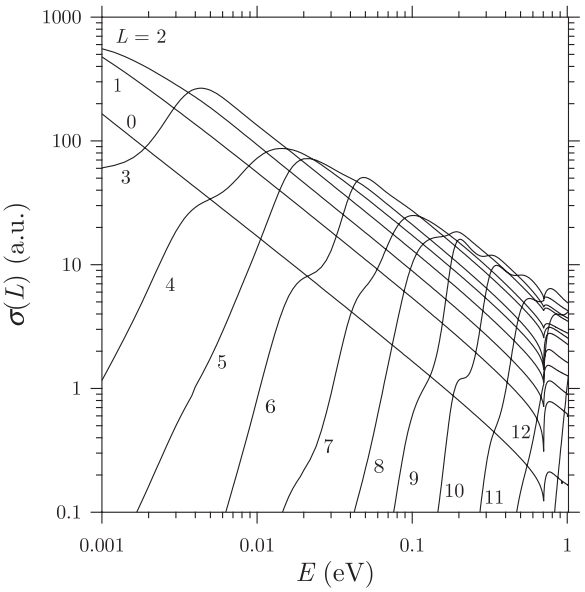

FIG. 6. L-state selected capture cross sections $\sigma(L)$ as a function of the collision energy E.

energy E. The most populated L state of $\mu^- p$ becomes higher in incremental steps as the energy increases. To explain the behavior of L_0 in more detail, we also plot the critical total angular momentum quantum number J_{max} in Fig. 7: At each collision energy E, the barrier height of the effective potential is below E for $J = J_{max}$ and is above E for $J = J_{max} + 1$ (cf. Fig. 1). The capture reaction is classically allowed only if $J \leqslant J_{max}$. We can see that L_0 is roughly equal to J_{max}. This result is evidently related to the fact that the total capture cross section is close to the Langevin value σ_L. These features are quite different from those seen in the μ^- capture by He^+ [13]. In this case, as a result of the long-range Coulomb attraction between μ^- and He^+, high angular momentum states of $\mu^- He^{2+}$ can be formed even at very low collision energies

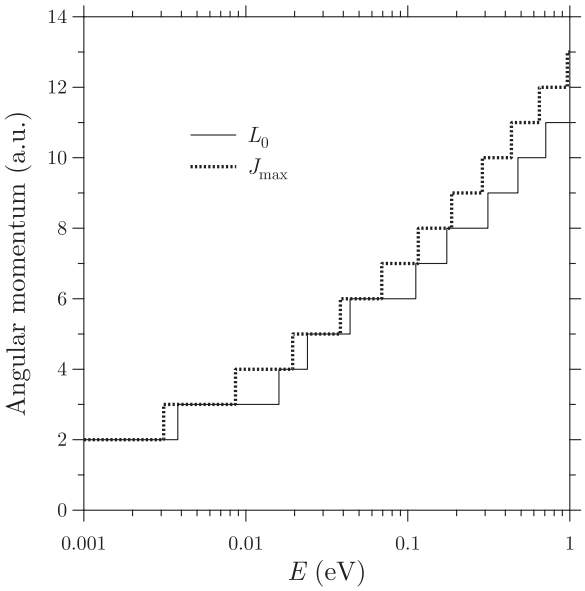

FIG. 7. Angular momentum quantum numbers L_0 and J_{max} (see text) as a function of the collision energy E.

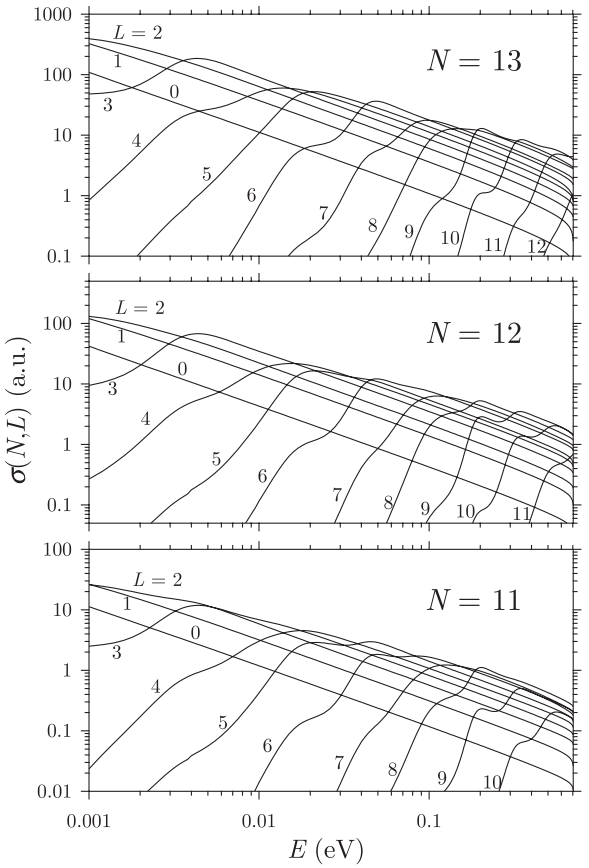

FIG. 8. (N, L)-state selected capture cross sections $\sigma(N, L)$ for $N = 11$, 12, and 13 as a function of the collision energy E.

and the most populated angular momentum state is always ~ 10 regardless of the energy if the resonance process does not take place.

The (N, L)-state selected capture cross sections $\sigma(N, L)$ are plotted against E in Fig. 8 for $N = 11$, 12, and 13. If we focus on the same L, the energy dependence of $\sigma(N, L)$ for every N looks very similar to that of $\sigma(L)$ except for the magnitude. We see that near circular states ($L \sim N - 1$) of $\mu^- p$ can be formed only at high energies. The further details about the L distribution specifically for the highest $N = 13$ state are shown at several energies in Fig. 9. As the energy decreases, the angular momentum has a narrower distribution centering around lower L. Even in the limit as $E \to 0$, not only the $L = 0$, but also the $L = 1$ state will be formed significantly. This is because the emission of electrons having $l = 0$ and 1 is always important in the capture process.

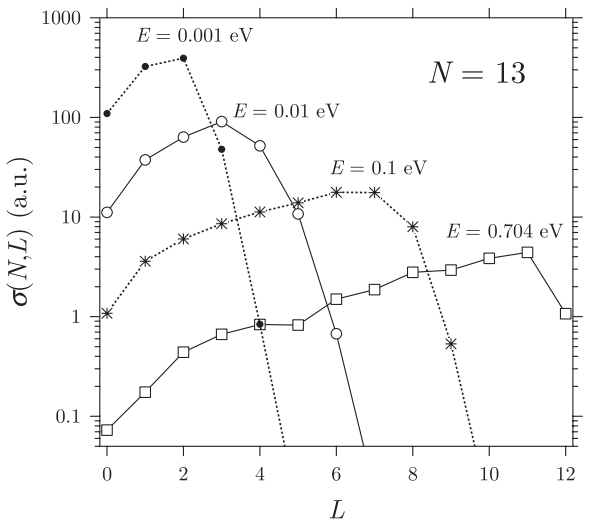

FIG. 9. (N, L)-state selected capture cross sections $\sigma(N, L)$ for $N = 13$ as a function of the angular momentum quantum number L at several collision energies E.

IV. SUMMARY AND FURTHER DISCUSSION

Using the R-matrix method, we carried out the QM calculations of the total and final-state selected cross sections for the μ^- capture by H in the region of collision energies $\leqslant 1$ eV.

The averaged total capture cross section is estimated to be about 0.79 times the Langevin value at very low collision energies. As the energy becomes high, the energy dependence deviates from that of the Langevin cross section. In this case, the empirical formula obtained in the previous study [9] is very useful for an estimate of the total capture cross section. The QM effect appears as an undulation around the value obtained by the empirical formula. The muons are dominantly captured into the highest energetically possible state of $\mu^- p$, almost regardless of the collision energy. However, the angular momentum distribution of $\mu^- p$ differs largely depending on the energy and only low angular momentum states can be formed at very low energies.

The empirical formula is available also for the $\bar{p}$ capture by H [8] and is expected to be useful for a rough estimate as well. However, it should be remembered that the s states of the product $\bar{p}p$ are quite unstable owing to the pair annihilation [5]. The annihilation energy width for the s state is estimated to be $1.06\bar{N}^{-3}$ keV [5], with $\bar{N}$ being the principal quantum number of $\bar{p}p$. The feature of the product-state distribution in the $\bar{p}$ capture will be qualitatively the same as that in the present case. Then, the most populated $\bar{p}p$ state in the $\bar{p}$ capture will be $\bar{N} = 30$ at low collision energies. For $\bar{N} = 30$, the s-state lifetime against annihilation becomes $\sim 2 \times 10^{-14}$ s, which is shorter than a typical time scale of a low-energy ion-molecule reaction. This means that the $\bar{p}p$ formation in the s state should not be counted as the effective capture process. The investigation of the low-energy collisions between $\bar{p}$ and H requires careful attention.

As was discussed in Ref. [17], the long-range dipole interaction between $\mu^- p$ and e and the hydrogenic degeneracy of $\mu^- p$ can support resonances just below the collision energy corresponding to the $\mu^- p$ excitation energy. Unfortunately, no such resonances can be found in the present calculation. A search for such resonances will require numerical computation with much more effort [17] and remains for future work.

ACKNOWLEDGMENTS

The present work was partially supported by the Grant-in-Aid for Scientific Research (C) from the Japan Society for the Promotion of Science.

[1] D. Taqqu *et al.*, Hyperfine Interact. **119**, 311 (1999).
[2] T. Nebel *et al.*, Can. J. Phys. **85**, 469 (2007).
[3] H.-Ch. Schröder *et al.*, Phys. Lett. **B469**, 25 (1999).
[4] M. Iwasaki *et al.*, Phys. Rev. Lett. **78**, 3067 (1997).
[5] E. Klempt, F. Bradamante, A. Martin, and J. M. Richard, Phys. Rep. **368**, 119 (2002).
[6] D. Gotta, Prog. Part. Nucl. Phys. **52**, 133 (2004).
[7] J. S. Cohen, Rep. Prog. Phys. **67**, 1769 (2004).
[8] K. Sakimoto, Phys. Rev. A **65**, 012706 (2001).
[9] K. Sakimoto, Phys. Rev. A **66**, 032506 (2002).
[10] X. M. Tong, K. Hino, and N. Toshima, Phys. Rev. Lett. **97**, 243202 (2006).
[11] X. M. Tong, T. Shirahama, K. Hino, and N. Toshima, Phys. Rev. A **75**, 052711 (2007).
[12] K. Sakimoto, Phys. Rev. A **76**, 042513 (2007).
[13] K. Sakimoto, Phys. Rev. A **80**, 012517 (2009).
[14] P. G. Burke and W. D. Robb, Adv. At. Mol. Phys. **11**, 143 (1976).
[15] E. Fermi and E. Teller, Phys. Rev. **72**, 399 (1947).
[16] A. S. Wightman, Phys. Rev. **77**, 521 (1950).
[17] K. Sakimoto, Phys. Rev. A **78**, 042509 (2008).
[18] C. Bloch, Nucl. Phys. **4**, 503 (1957).
[19] M. Gailitis and R. Damburg, Proc. Phys. Soc. **82**, 192 (1963).
[20] T. F. O'Malley, Phys. Rev. **137**, 1668 (1965).
[21] R. S. Friedman and D. G. Truhlar, Chem. Phys. Lett. **183**, 539 (1991).
[22] F. T. Smith, Phys. Rev. **118**, 349 (1960).